Proceedings Paper:
John, E., Boxall, J., Collins, R. et al. (2024) Experimental validation of a model for predicting the bending fatigue strength of corroded grey cast iron water pipes. In: Proceedings of the 9th Engineering Integrity Society International Conference on Durability & Fatigue. Fatigue 2024: 9th Engineering Integrity Society International Conference on Durability & Fatigue, 19-21 Jun 2024, Cambridge, UK. Engineering Integrity Society, pp. 482-493. ISBN: 9780954436872.

EXPERIMENTAL VALIDATION OF A MODEL FOR PREDICTING THE BENDING FATIGUE STRENGTH OF CORRODED GREY CAST IRON WATER PIPES

Edward John[1], Joby Boxall[1], Richard Collins[1], Elisabeth Bowman[1], & Luca Susmel[1]

Leakage of drinking water caused by mechanical failures of old, buried, Grey Cast Iron (GCI) water pipes is a serious issue for water utilities in the UK and around the world. To enable better-informed pipe health assessments to be made, this work aimed to experimentally validate a method that could be used to assess the damaging effect of corrosion pitting on GCI pipes subject to bending fatigue loading. Fatigue testing of GCI pipes revealed pitting had a small detrimental effect on the pipes' bending fatigue strength, characterised by K_t = 1.38 for the sharp pit specimens. An effective volume approach coupled with the SWT multiaxial fatigue criterion was found to provide reasonable fatigue life predictions, at the expense of requiring the 3D geometry of the pit to be known. Making predictions simply using the net stresses provided conservative predictions, but only required the pit's depth.

Keywords: Metal fatigue, Life prediction, Notch fatigue, High-cycle fatigue

INTRODUCTION

The UK water industry has committed to halving leakage rates by 2050, compared to 2017/18 levels, which will require targeted pipe replacement (Sanders at al., [1]). To decide which pipes to replace one must be able to assess the relative health of a given pipe. Grey Cast Iron (GCI) pipes are one of the oldest and most common pipe materials in use in the UK (Barton et al., [2]). GCI pipes also have high failure rates per km compared to other pipe materials in use in the UK [2], making assessing the health of the remaining GCI pipes a priority. The damp, aerated conditions found in the soil surrounding many buried GCI water pipes promotes the growth of corrosion pitting on the external surface of the pipes (Logan et al., [3]). The corrosion process replaces the original iron with a much weaker corrosion product, which is often modelled as a pit in the pipe wall for structural analysis (Atkinson et al., [4] and Zhang et al., [5]). As a result, corrosion pitting can act as a notch, concentrating stress in the pipe wall and causing cracks for form under loading that would not damage an un-corroded pipe [5].

Small diameter GCI water pipes are commonly found to have developed circumferential cracks, which are usually attributed to bending loads [2]. Many pipes are buried under roads, so a common source of bending load is vehicle loading (Randeniya et al., [6]). The time variable nature of vehicle loading means small diameter pipes may develop leaking cracks due to bending fatigue loading. No validated models are available that can predict the damaging effect of corrosion pitting on the fatigue strength of GCI pipes subject to bending loads (Brevis et al., [7] and Jiang et al., [8]). This means asset managers are unable to accurately assess the damaging effect of corrosion pitting on the GCI pipes they are responsible for, impeding their ability to make asset health assessments.

[1]Department of Civil and Structural Engineering, The University of Sheffield, Sheffield, UK

GCI is often credited with very low fatigue notch sensitivity (Pilkey and Pilkey, [9]). The available notch fatigue data for GCI is limited, covering only solid cylindrical specimens with sharp circumferential V-notches under uniaxial and rotating bending loads (Taylor et al., [10] and Lampman, [11]). This data is limited in its relevance to corrosion pitting in GCI pipes where localised, blunt notches are common, and the material depth behind the notch may be a couple of mm or less [5]. Data quoted by Heywood [12] for several different GCIs give bending fatigue strengths 1.38 to 1.69 times higher than the axial fatigue strength. No data is available for bending fatigue of notched GCI.

To predict the fatigue strength of notched GCI, Heywood [12] proposed an empirical equation that predicts the fatigue strength reduction factor based on the stress concentration factor, notch root radius, and a material parameter equal to the length of equivalent internal flaws. Heywood's equation has not been validated for notch geometries representative of corroded GCI pipes. The notch fatigue behaviour of GCI is thought to be controlled by the distribution of its internal flaws [9]. The effective volume approach to notch fatigue was developed by Bomas et al. [13] to account for the interaction between stress gradients and a material's internal defect distribution. The effective volume approach therefore has potential to capture the notch fatigue behaviour of GCI, however it has not been validated for GCI.

The stress histories experienced by in-service GCI water pipes due to vehicle loading typically feature non-zero mean stresses [6]. Additionally, notches can create localised multiaxial stress fields [9]. Fash and Socie [14] found that the Smith-Watson-Topper (SWT) criterion was also able to account for the mean stress effect for GCI in the HCF regime, and more recently John et al. [15] found that the SWT criterion was also able to predict the un-notched multiaxial fatigue behaviour of GCI.

The work detailed in this paper aimed to experimentally validate a method that can be used to assess the damaging effect of corrosion pitting on GCI pipes subject to bending fatigue loading. In this study, corrosion pitting was assumed to be analogous to notches in a pipe's wall. To investigate the interaction between notch geometry and bending loading, notched and un-notched specimens were tested under uniaxial and bending loading. In order to identify the most effective prediction method the following approaches were used to predict the observed fatigue data: the net stress amplitude; Heywood's equation; the effective volume in terms of maximum principal stress amplitude; and the effective volume in terms of the SWT criterion equivalent stress amplitude.

METHODS

Uniaxial fatigue tests

To investigate effect of notch sharpness on fatigue strength two designs of circumferentially notched uniaxial specimens were tested: one with a sharp 0.4 mm root radius and 35° flank angle and one with a blunt 5.0 mm root radius. The specimens were manufactured from the same DN50 BS416-2 [16] GCI pipes as the specimens tested by [15] to allow direct comparison of results. The remaining wall thickness behind the notch root was approximately 1.8 mm for all specimens.

To characterise the fatigue curves of these specimens, 10 specimens were tested across 5 stress levels, giving 50% replication. Tests were run under load control at 8 Hz and $2x10^6$ cycles was used as the runout definition. Due to the rapid crack propagation observed, failure was defined as specimen separation, as shown by Figure 1.

a) Sharp notch uniaxial specimen

b) Blunt notch uniaxial specimen

FIGURE 1 Examples of failed (a) sharp and (b) blunt notch uniaxial fatigue specimens.

a) Un-notched bending specimen b) Sharp notch bending specimen

FIGURE 2 Examples of failed bending specimens.

Bending fatigue tests

The un-notched bending specimens (Figure 2a) featured a gauge section with a large transition radius to ensure failure occurred in the centre of the specimen. To represent realistic corrosion pitting more closely than the uniaxial specimens, the notched bending specimens had local, axisymmetric notches drilled into them, as shown by Figure 2b. Two designs of notched bending specimens were tested: one with a sharp 0.1 mm root radius, 90° flank angle notch, and one with a blunt 4 mm root radius notch. The bending specimens were also manufactured from DN50 BS416-2 [16] pipes. The remaining wall thickness at the gauge section of the un-notched bending specimens and behind the notch roots of the notched bending specimens was also 1.8 mm.

So that failures would occur in a region of uniform bending stress away from the influence of the load points, the bending specimens were tested under four-point bending. Deformation of the pipe cross section was minimised by using saddle-shaped supports and load points. Real-world bending fatigue loading of small diameter pipes is likely to feature a mean stress, so a load ratio of 0.1 was used for all bending fatigue tests. This also facilitated comparison with the un-notched uniaxial R = 0.1 fatigue data from [15].

The bending fatigue tests aimed to provide data against which the models could be tested, as well as characterise approximate slope and position of the SN curves. Therefore, four specimens were tested across two stress levels. Tests were run under load control at 4 Hz and $6x10^5$ cycles was used as the runout definition as very few uniaxial failures occurred after this number of cycles. Specimen separation was used to define failure.

Fatigue data analysis

The net stresses applied to the uniaxial specimens were calculated as the applied force divided by the net area. The net and gross stresses applied to the bending specimens were determined using the Finite Element Analysis (FEA) procedure described below.

The least squares method was used to estimate the relationship between stress amplitude and cycles to failure according to ASTM E739-10 [17] for each loading type, except the blunt notch results as these did not give a clear linear relationship. The least squares estimate is the 50% probability of survival estimate (P_S=50%). The 10% and 90% probability of survival scatter bands were calculated at a 95% confidence level for the un-notched uniaxial data according to ASTM STP91 [18]. Scatter bands were not calculated for the other data sets because they contained insufficient data points.

Notch fatigue strength predictions

To test the idea that the material is insensitive to notch geometry fatigue life predictions were made using the net stress amplitude. The area used to calculate the net stress for the notched bending specimens was determined by assuming that all material above deepest point of pit was removed. To make fatigue life predictions the net stress amplitude applied to each specimen was compared to the un-notched uniaxial R=-1 and R=0.1 P_S=50% curves from [15].

Heywood's equation for GCI is given by:

$$K_f = \frac{K_t}{1+2\left(\frac{K_t-1}{K_t}\right)\left(\frac{a'}{r}\right)^{1/2}} \quad (1)$$

where: K_f is the fatigue strength reduction factor; K_t is the stress concentration factor; r is the notch root radius (mm); and a' is the material notch alleviation factor (mm). To make predictions using Heywood's equation K_t values were calculated for each specimen design using FEA. The uniaxial sharp notch data was used to calibrate Heywood's equation, giving a' = 1.53 mm. K_f calculated for each notched specimen type is given in Table 1. The un-notched uniaxial R=-1 and R=0.1 P_S=50% curves from [15] were modified using these K_f values and used to make fatigue life predictions.

Using the effective volume approach of Bomas et al. [13] the fatigue limit of a given geometry and load type, σ_A, in terms of maximum linear elastic stress is calculated as follows:

$$\sigma_A = \sigma_{A,0}\left(\frac{V_{eff,0}}{V_{eff}}\right)^{1/m} \quad (2)$$

where: $\sigma_{A,0}$ is the fatigue limit of the reference condition in terms of maximum linear-elastic stress; $V_{eff,0}$ is the effective volume of the reference condition; V_{eff} is the effective volume of the condition of interest; and m is a material parameter which is a function of the defect size distribution and fracture mechanics properties of the material. For a given geometry and load condition, the effective volume is calculated as follows [13]:

$$V_{eff} = \int_V \left(\frac{\sigma_a(x,y,z)}{\sigma_{a,max}}\right)^m dV \quad (3)$$

where: σ_a is the stress amplitude at any coordinate point x, y, z within the material; and $\sigma_{a,max}$ is the maximum stress amplitude occurring at any point within the material. The stress amplitude used in Equations 2 and 3 may be a principal stress amplitude, or the amplitude of an equivalent stress [13]. To test the effective volume approach with and without consideration for multiaxial notch stresses the effective volume approach was applied in terms of maximum principal stress amplitude and in terms of the SWT equivalent stress, given by Dowling et al. [19] as:

$$\sigma_{a,SWT} = \sqrt{\sigma_{n,max} E \varepsilon_{n,a}} \quad (4)$$

where: $\sigma_{a,SWT}$ is the SWT equivalent fully reversed stress amplitude; $\sigma_{n,max}$ is the maximum value of normal stress on the critical plane; E is the material's elastic modulus; and $\varepsilon_{n,a}$ is the normal strain amplitude on the critical plane. The critical plane is that experiencing the maximum value of $\varepsilon_{n,a}$.

To calculate V_{eff} for each specimen geometry according to Equation 3, the material constant, m, had to be determined. Since FEA results are divided into discrete element volumes V_{eff} was approximated as:

$$V_{eff} = \sum_{i=1}^{n} \left[\left(\frac{\sigma_{a,i}}{\sigma_{a,max}}\right)^m V_i\right] \quad (5)$$

where: n is the number of elements in the FEA model; $\sigma_{a,i}$ is the stress amplitude experienced by element i; $\sigma_{a,max}$ is the greatest stress amplitude experienced by any element the FEA model; and V_i is the volume of element i. Through a trial and improvement process, m was found such that Equation 2 was able to accurately predict the sharp notch uniaxial fatigue P_S=50% curve, using the un-notched uniaxial R = -1 curve as the reference condition. The value of m calculated using the first principal stress amplitude was 6.30, and 6.74 was calculated using the SWT equivalent stress. Values of V_{eff} were calculated with these values of m for all other geometries using Equation 5 (see Table 1), and cycles to failure predictions were made for each data set by constructing an SN curve with the negative inverse slope of the reference curve and the high-cycle reference stress amplitude calculated using Equation 2. For the effective volume approach in terms of principal stress amplitude, mean stress was accounted for using the approach described above for Heywood's equation. The prediction accuracy of each approach was quantified using the mean square error quantity, T_{RMS}, as detailed by Walat and Lagoda [20].

Finite element analysis

To calculate K_t and V_{eff} for each specimen type linear-elastic FEA was used. Because the bending specimens displayed some cross-sectional deformation at the load points FEA was also used to determine the gross and net stresses in these specimens, instead of classical beam theory.

For computational efficiency, the uniaxial specimens were modelled as axisymmetric problems. The bending specimens required three-dimensional models, although the size of these was reduced by taking advantage of two planes of symmetry. The boundary conditions of the bending specimen FEA were significantly more complex than the uniaxial specimen analysis, so the bending models were validated against strain-gauge and LVDT measurements. The bending models were able to predict the strain and displacement measurements to within ±10%. The mesh was refined in the critical region of each model until the volume of elements experiencing 95% of the maximum principal stress converged to within 10%. V_{eff} was not used to determine convergence because V_{eff}

= f(m), and m is determined iteratively. Element sizes that achieved convergence varied between 0.2 mm for the un-notched specimens and 0.001 mm for the sharp notched specimens.

TABLE 1 Parameters used to make predictions for the data sets.

Specimen type	**Stress type**	**Notch root radius (mm)**	**K_t**	**Heywood K_f**	**σ_1 V_{eff} (mm^3)**	**SWT V_{eff} (mm^3)**
Uniaxial un-notched	-	-	1.02	-	$1.40x10^4$	$1.32x10^4$
Uniaxial sharp notch	Net	0.4	4.74	1.12	$2.09x10^0$	$1.63x10^0$
Uniaxial blunt notch	Net	5.0	2.14	1.33	$5.85x10^1$	$5.03x10^1$
Bending un-notched	-	-	1.01	-	$1.67x10^3$	$1.43x10^3$
Bending sharp notch	Gross	0.1	3.85	0.57	$2.28x10^{-1}$	$1.45x10^{-1}$
Bending blunt notch	Gross	4.0	2.14	1.29	$1.55x10^1$	$2.34x10^1$

RESULTS

Examples of failed uniaxial and bending specimens are shown by Figures 1 and 2, respectively. The fracture surface was perpendicular to the maximum principal stress amplitude direction in all cases.

The uniaxial specimen fatigue data are plotted in Figure 3 in terms of net stress, along with the P_s = 50% line for the sharp notch specimens. The P_s = 50% line was not calculated for the blunt notch uniaxial data because data was not available for a sufficient range of stress levels to give a reasonable estimation of the slope. This is because the blunt notch specimens survived $2x10^6$ load cycles at relatively high stress amplitudes (see Figure 3). All but one of the uniaxial notched results fell within the 10%-90% probability of survival scatter bands of the un-notched data set.

The bending specimen fatigue data are plotted in Figure 4, along with the P_s = 50% lines for the un-notched and sharp notch specimens. The un-notched bending specimen stresses plotted were calculated from the gauge cross-section. Because the notches only caused a small reduction in cross-sectional area for the notched bending specimens, the applied gross stresses are plotted. Like the blunt notch uniaxial specimens, the blunt notch bending specimens survived $6x10^5$ cycles at relatively high stress amplitudes (see Figure 4) so the range of stress levels tested with these specimens was too small to give a reasonable estimation of the P_s = 50% line slope.

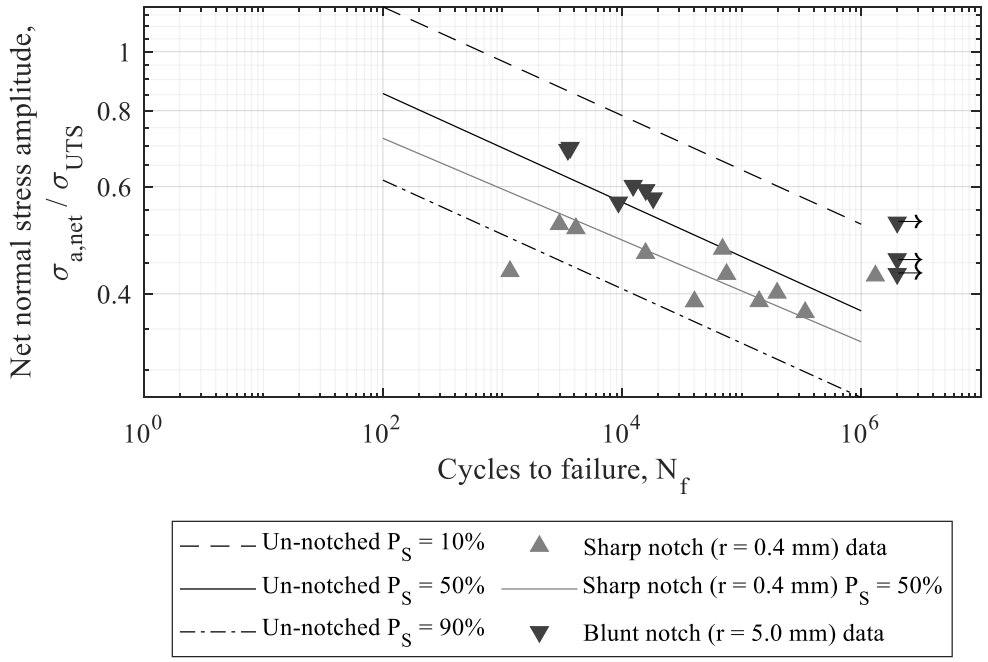

FIGURE 3 Fatigue data and fitted curves for notched specimens under R = -1 uniaxial loading. The un-notched uniaxial fatigue curve and scatter bands from [15] are provided for reference.

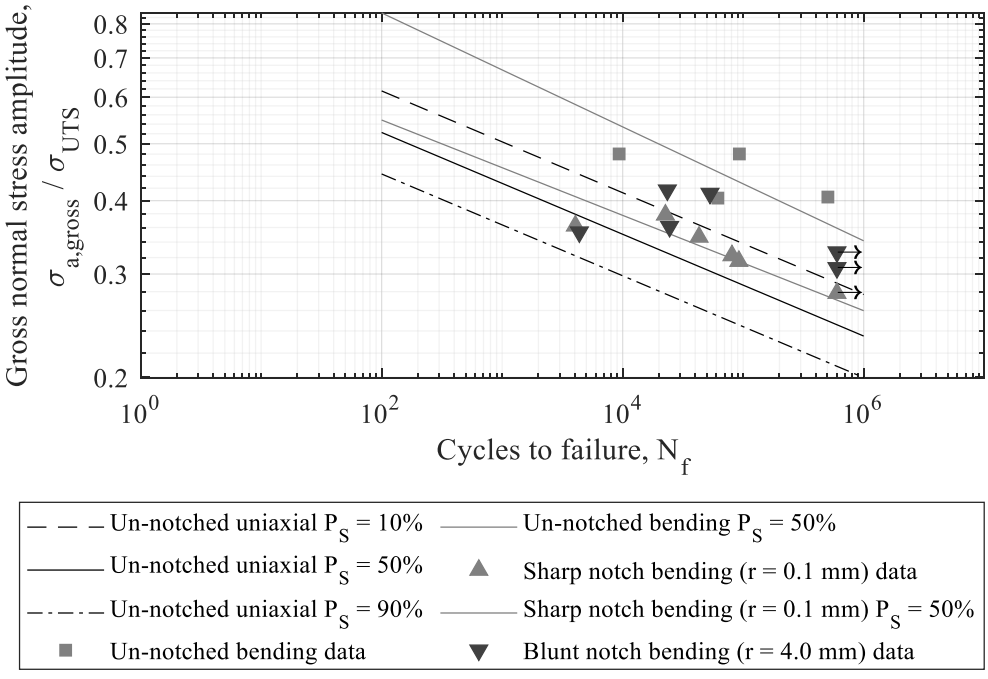

FIGURE 4 Fatigue data and fitted curves for un-notched and notched bending specimens under R = 0.1 loading. The un-notched uniaxial fatigue curve and scatter bands from [15] are provided for reference.

The predicted fatigue life vs measured fatigue life are plotted for each prediction method in Figure 5. Note that the predictions made by Heywood's equation for the sharp notch bending data all exceeded 10^8 cycles and so are not included in Figure 5. The prediction accuracy of each method in terms of T_{RMS} is given in Table 2.

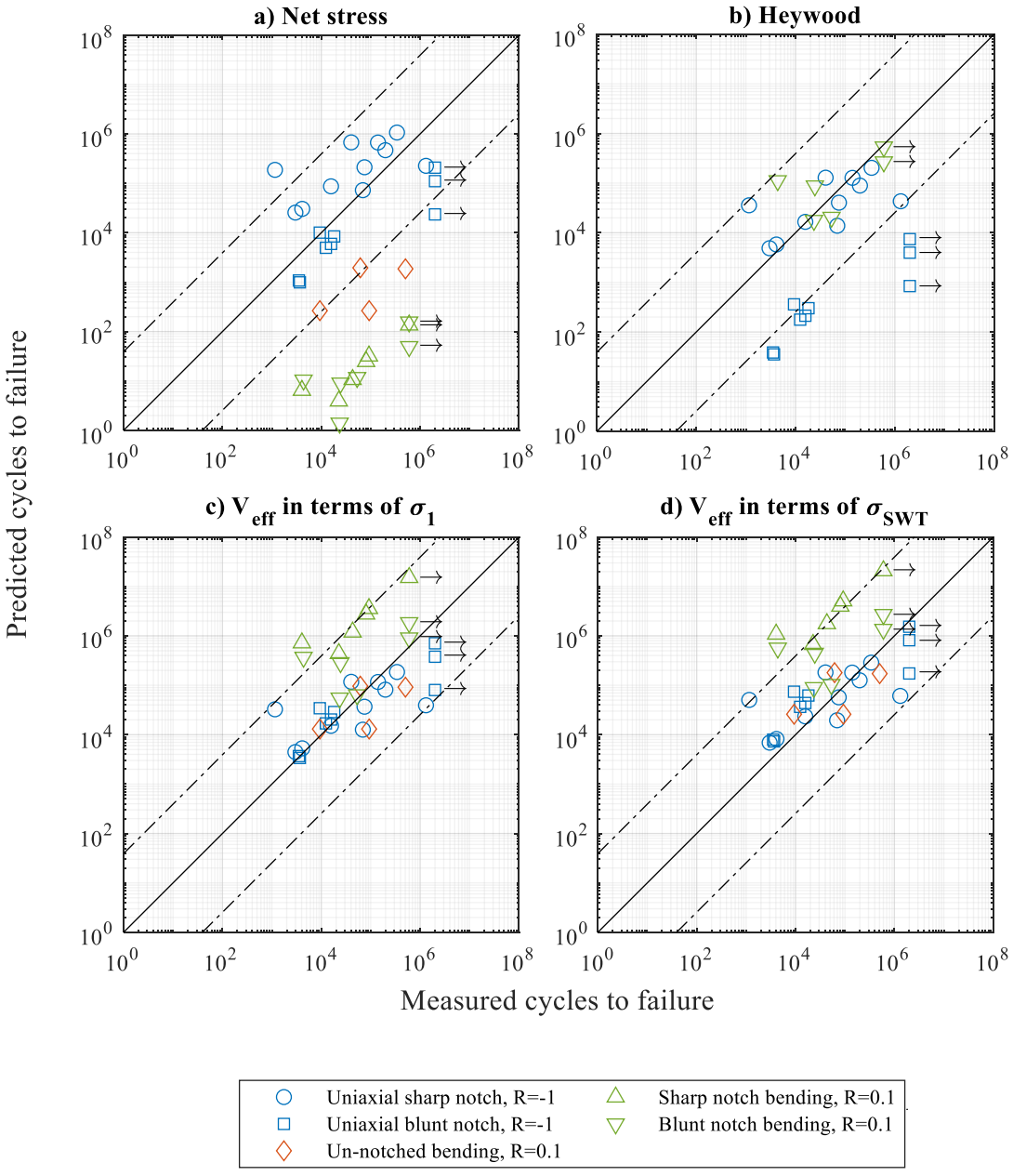

FIGURE 5 Predicted cycles to failure vs measured cycles to failure for the notch fatigue strength prediction methods. Dashed lines show the fully reversed uniaxial scatter band from [15].

TABLE 2 Prediction effectiveness measured using T_{RMS} with the lowest (best) values for each data set highlighted in **bold**.

Data set	Prediction T_{RMS}			
	Net stress	**Heywood's equation**	**V_{eff} in terms of σ_1**	**V_{eff} in terms of σ_{SWT}**
Uniaxial, R = -1, sharp notch	**9.18**	-	-	-
Uniaxial, R = -1, blunt notch	2.61	66.71	**1.80**	3.44
Bending, R = 0.1, un-notched	116.10	-	3.78	**3.05**
Bending, R = 0.1, sharp notch	2.78×10^3	4.93×10^4	**45.10**	66.11
Bending, R = 0.1, blunt notch	3.40×10^3	6.11	**13.10**	18.68

DISCUSSION

To establish whether the GCI specimens tested for this work demonstrated a similar response to the available literature data, the sharp notch uniaxial data and un-notched bending data were compared with literature data. The low notch sensitivity of the sharp notch uniaxial specimens (Figure 3) was consistent with the experimental observations made by [10] and reported by [11] for similar specimens. Specifically, the fatigue notch sensitivity (q) value for the sharp notch uniaxial specimens was calculated as 0.03 which falls within the lower end of the 0.00 to 0.27 range of q values reported by the above authors. In the absence of pitting, bending fatigue loading was less damaging to the GCI pipes than uniaxial fatigue loading. All the un-notched bending fatigue data points fell outside the scatter bands of the uniaxial data (Figure 4), indicating the significance of this effect. In terms of high-cycle reference stress amplitudes, the bending fatigue strength of the material was 1.49 times higher than the axial fatigue strength, which falls within the 1.38 to 1.69 range reported by [12] for grey cast irons. The sharp notch uniaxial data and un-notched bending data generated by this work are therefore comparable to other data sets for the material.

The blunt notch uniaxial specimen data (Figure 3) indicated the blunt notch did not reduce the fatigue strength of the specimens whatsoever. Curiously, runouts occurred for this specimen type at much higher stress amplitudes than for the sharp notch uniaxial specimens suggesting the knee-point of the fatigue curve was affected by the notch root radius. Turning to the more realistic notched bending data, Figure 4 shows that the localised notches reduced the fatigue strength of the GCI pipes subject to bending loading, relative to the un-notched specimens under bending loads, and the sharper notches had a slightly more detrimental effect than the blunt notches. Specifically, the fatigue strength of the sharp notch specimens under bending loading was 1.38 times lower than the un-notched specimens, giving q = 0.13. These results show that GCI has some sensitivity to notch sharpness and to the presence of localised notches under bending fatigue loading.

As shown by Figure 5 and Table 2, the fatigue strength predictions made using the net stress gave good predictions for the uniaxially loaded notched data, but very conservative predictions for the pipes under bending loads. A benefit of this approach is that the only information required about the corrosion pitting is its depth, making it easier to apply in the field. For practical applications, such as selecting pipes for replacement, very conservative predictions are safer than very non-conservative predictions. Heywood's equation gave very inconsistent predictions and was therefore unable to capture the effect of notch root radius on the fatigue strength of GCI pipes under bending loading.

The effective volume approach applied in terms of principal stress amplitude provided good predictions for the uniaxially loaded notched data and the un-notched bending data. The predictions for the notched bending data were reasonable but verged on being non-conservative (see Figure 5). The effectiveness of this approach indicates that the higher un-notched bending fatigue strength of the material can be attributed to the fact that a smaller volume of a bending specimen experiences the highest stress amplitude. The coupled effective volume and SWT multiaxial fatigue criterion provided similar predictions for the notched and un-notched bending data to the effective volume approach referencing the uniaxial R = 0.1 SN curve (see Table 2). This indicates that, for the specimens tested, local multiaxial stresses caused by the notches had a small effect on the predicted fatigue strength. Combining the effective volume and SWT multiaxial fatigue criterion gives a tool that has the potential to make reasonable fatigue life predictions for pitted GCI pipes under a range of load ratios, although further tests under other load ratios and notch geometries would be required to confirm this.

In terms of practical application, the effective volume approach requires the full 3D geometry of a corrosion pit and considerable computing power to calculate the effective volume. This makes the effective volume approach ill-suited to in-field application to specific buried pipes. However, the ability of the effective volume approach to capture the effect of pitting on the fatigue strength of the material means that it could act as a useful tool to assess the relative effect of different forms of corrosion, and potentially identify limits to the net stress approach with fewer experiments.

CONCLUSIONS

This work aimed to experimentally validate a method that can be used to assess the damaging effect of corrosion pitting on GCI pipes subject to bending fatigue loading, motivated by the need to assess the damaging effect of corrosion pitting on GCI water pipes. The following conclusions were drawn:

- Localised surface pits have a small detrimental effect on the bending fatigue strength of GCI pipes, characterised by $K_t = 1.38$ for the sharp notch specimens tested, and the material demonstrates some sensitivity to notch root radius.
- Making fatigue life predictions using the net principal stress amplitude provides a simple but very conservative approach to predicting the damaging effect of corrosion pits on the fatigue strength of GCI pipes subject to bending loading.
- The effective volume approach coupled with the SWT multiaxial fatigue criterion can make reasonable fatigue life predictions for notched GCI pipes subject to bending fatigue loading. A limitation of this approach for in-field use is the fact that the three-dimensional geometry of a corrosion pit is required as an input, which is difficult information to obtain for buried pipes.

LIST OF SYMBOLS

a'	Material notch alleviation factor.	T_{RMS}	Mean square error.
E	Elastic modulus.	V	Volume.
i	FEA element number.	V_{eff}	Effective volume of the condition of interest.
K_t	Stress concentration factor.	$V_{eff,0}$	Effective volume of the reference condition.
K_f	Fatigue strength reduction factor.	$\varepsilon_{n,a}$	Normal strain amplitude.
m	Effective volume material constant.	σ_A	High-cycle reference stress amplitude of the condition of interest.
n	FEA number of elements.	$\sigma_{A,0}$	High-cycle reference stress amplitude of the reference condition.
P_S	Probability of survival.	σ_a	Stress amplitude.
q	Fatigue notch sensitivity: $q = (K_f-1)/(K_t-1)$	$\sigma_{a,SWT}$	SWT equivalent stress amplitude.
R	Fatigue load ratio: $R = \sigma_{min}/\sigma_{max}$	$\sigma_{n,max}$	Maximum normal stress.
r	Notch root radius.		

REFERENCE LIST

(1) Sanders, J., Marshallsay, D., Mountfort, G., Fox, G., and Butler, M., A *leakage routemap to 2050*, Water UK, London, UK, 2022.

(2) Barton, N. A., Farewell, T. S., Hallett, S. H., and Acland, T. F., *Water Res.*, Vol. **164**, 2019.

(3) Logan, R., Mulheron, M. J., Jesson, D. A., Smith, P. A., Evans, T. S., Clay-Michael, N., and Whiter, J. T., *WIT Trans. on The Built Env.*, Vol. **139**, 2014, pp. 411–422.

(4) Atkinson, K., Whiter, J. T., Smith, P. A., and Mulheron, M., *Urban Water*, Vol. **4**, 2002 pp. 263–271.

(5) Zhang, C., Rathnayaka, S., Shannon, B., Ji, J., and Kodikara, J., I*nt. J. Mech. Sc.*, Vol. **128**, 2017, pp. 116–124.

(6) Randeniya, C., Robert, D.J., Li, C-Q., and Kodikara, J., *Canadian Geotech. J.*, Vol. **57**, 2020, pp. 205–220.

(7) Brevis, W., Susmel, L., and Boxall, J., *Proc. Inst. Mech. Eng. C J. Mech. Eng. Sc.*, Vol. **229**, 2015, pp. 1240–1259.

(8) Jiang, R., Rathnayaka, S., Shannon, B., Zhao, X-L., Ji, J., and Kodikara, J., *Eng. Fail. Anal.*, Vol. **103**, 2019, pp. 238–248.

(9) Pilkey, W. D., and Pilkey, D. F., *Peterson's stress concentration factors*, John Wiley & Sons, Inc., Hoboken, N.J., 2008.

(10) Taylor, D., Hughes, M., and Allen, D., *Int. J. Fatigue*, Vol. **18**, 1996, pp. 439–445.

(11) Lampman, S, *Fatigue and fracture properties of cast irons*, ASTM Int., U.S.A., ASM Handbook, Volume 19: Fatigue and Fracture, 1996.

(12) Heywood, R. B., *Designing against fatigue*, Chapman Hall Ltd., London, UK, 1962.

(13) Bomas, H., Linkewitz, T., and Mayr, P., *Fatigue Fracture Eng. Mater. Struct.*, Vol. **22**, 1999, pp. 733–741.

(14) Fash, J., and Socie, D. F., *Int. J. Fatigue*, Vol. **4**, 1982, pp. 137–142.

(15) John, E., Boxall, J., Collins, R., Bowman, E., and Susmel, L., *Int. J. Fatigue*, Vol. **178**, 2024.

(16) BSI, *Discharge and ventilating pipes and fittings, sand-cast or spun in cast iron - part 2: Specifications for socketless systems*, BS 416-2:1990, British Standards Publications, London, UK, BS 416-2:1990, 1990.

(17) ASTM, *Standard Practice for Statistical Analysis of Linear or Linearized Stress-Life (S-N) and Strain-Life (ε-N) Fatigue Data*, ASTM Int., U.S.A., ASTM E739-10, 2015.

(18) ASTM, *A guide for fatigue testing and the statistical analysis of fatigue data*, ASTM Int., U.S.A., ASTM STP 91, 1963.

(19) Dowling, N., Calhoun, C., and Arcari, A., *Fatigue Fracture Eng. Mater. Struct.*, Vol. **32**, 2008, pp. 163–179.

(20) Walat, K., and Lagoda, T., *Int. J. Fatigue*, Vol. **67**, 2014, pp. 73–77.